

University of Groningen

## Multisided generalisations of Gregory patches

Hettinga, Gerben J.; Kosinka, Jiri

*Published in:*  
Computer aided geometric design

*DOI:*  
[10.1016/j.cagd.2018.03.005](https://doi.org/10.1016/j.cagd.2018.03.005)

**IMPORTANT NOTE: You are advised to consult the publisher's version (publisher's PDF) if you wish to cite from it. Please check the document version below.**

*Document Version*  
Publisher's PDF, also known as Version of record

*Publication date:*  
2018

[Link to publication in University of Groningen/UMCG research database](#)

*Citation for published version (APA):*  
Hettinga, G. J., & Kosinka, J. (2018). Multisided generalisations of Gregory patches. *Computer aided geometric design*, 62, 166-180. <https://doi.org/10.1016/j.cagd.2018.03.005>

### Copyright

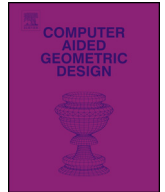
Other than for strictly personal use, it is not permitted to download or to forward/distribute the text or part of it without the consent of the author(s) and/or copyright holder(s), unless the work is under an open content license (like Creative Commons).

The publication may also be distributed here under the terms of Article 25fa of the Dutch Copyright Act, indicated by the "Taverne" license. More information can be found on the University of Groningen website: <https://www.rug.nl/library/open-access/self-archiving-pure/taverne-amendment>.

### Take-down policy

If you believe that this document breaches copyright please contact us providing details, and we will remove access to the work immediately and investigate your claim.

*Downloaded from the University of Groningen/UMCG research database (Pure): <http://www.rug.nl/research/portal>. For technical reasons the number of authors shown on this cover page is limited to 10 maximum.*



# Multisided generalisations of Gregory patches

Gerben J. Hettinga<sup>\*</sup>, Jiří Kosinka



Johann Bernoulli Institute, University of Groningen, 9747 AG Groningen, The Netherlands

## ARTICLE INFO

### Article history:

Available online 22 March 2018

### Keywords:

Multisided Bézier patches  
Gregory patches  
Local interpolation  
Generalised barycentric coordinates

## ABSTRACT

We propose two generalisations of Gregory patches to faces of any valency by using generalised barycentric coordinates in combination with two kinds of multisided Bézier patches. Our first construction builds on S-patches to generalise triangular Gregory patches. The local construction of Chiyokura and Kimura providing  $G^1$  continuity between adjoining Bézier patches is generalised so that the novel Gregory S-patches of any valency can be smoothly joined to one another. Our second construction makes a minor adjustment to the generalised Bézier patch structure to allow for cross-boundary derivatives to be defined independently per side. We show that the corresponding blending functions have the inherent ability to blend ribbon data much like the rational blending functions of Gregory patches. Both constructions take as input a polygonal mesh with vertex normals and provide  $G^1$  surfaces interpolating the input vertices and normals. Due to the full locality of the methods, they are well suited for geometric modelling as well as computer graphics applications relying on hardware tessellation.

© 2018 Elsevier B.V. All rights reserved.

## 1. Introduction

The creation of  $G^1$  (or tangent plane) continuous surfaces from a polygonal mesh has long been a problem in computer graphics and geometric modelling. Attaining this level of continuity locally, by using information from only one polygon at a time, is a difficult problem. By augmenting the positional data of the mesh with vertex normals it becomes possible to assure  $G^1$  continuity between adjacent patches by taking into account only locally defined information. Complex smooth shapes are easily modelled by automatically generating patches based on coarse polygonal meshes. In addition, such techniques are well suited for applications in computer graphics relying on hardware tessellation.

This work describes the augmentation of the S-patch structure (Loop and DeRose, 1989) with Gregory terms and rational blending functions. Moreover, the method of Chiyokura and Kimura (1983) is generalised to multisided faces such that a Gregory S-patch can be joined smoothly to adjacent (Gregory or Bézier) patches. The combination of these results in a multisided generalisation of triangular Gregory patches. In addition, the method of Chiyokura and Kimura is also applied to generalised Bézier patches (Várady et al., 2016). By adjusting the control point structure of this patch it becomes possible to define cross-boundary derivatives independently per side. This effectively creates a multisided generalisation of quadrilateral Gregory patches.

<sup>\*</sup> Corresponding author.

E-mail address: [g.j.hettinga@rug.nl](mailto:g.j.hettinga@rug.nl) (G.J. Hettinga).

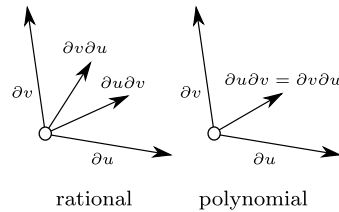


Fig. 1. In the rational case, mixed partial derivatives can be distinct, whereas in the polynomial case mixed partial derivatives are equal.

$G^1$  continuity is a less strict version of the parametric  $C^1$  continuity. Essentially, it means that along the shared boundary of two parametric surfaces the surface normal field is shared as well. When considering the problem of joining patches with  $G^1$  continuity, some difficulties arise. It is often the case when using polynomial constructions that cross-boundary derivatives can be matched on each one of the boundary edges separately, but internally the mixed partial derivatives,  $\partial u\partial v$  and  $\partial v\partial u$ , cannot (see Fig. 1). This is known as the vertex inconsistency problem or the twist compatibility problem. A commonly used solution is to employ rational functions that blend the derivatives accordingly.

Multisided surface patches are well-established in computer graphics and geometric modelling. They offer the ability to smoothly interpolate data over polygonal domains such that visually pleasing surface patches are created. However, the problem of how to smoothly join several of these patches together has not been given much attention. One such multisided patch is the S-patch (Loop and DeRose, 1989), which is a multisided generalisation of ordinary Bézier patches. In Section 3 the conditions of  $G^1$  continuity for S-patches are reviewed and it is shown how Chiyokura and Kimura's method can be adapted to S-patches. We first look at quadrilaterals (Section 3.1) and then show how the structure generalises to arbitrary polygons (Section 3.2).

Another representation of multisided surfaces was developed by Várady et al. (2016). This multisided patch, called the generalised Bézier patch, has a very compact structure compared to S-patches and combines transfinite and control point oriented structures. Section 4.1 shows how the structure of the generalised Bézier patch can be adjusted such that it blends ribbons in a Gregory-like manner and guarantees  $G^1$  continuity between adjacent patches.

We then present and discuss results obtained by the two methods (Section 5) and conclude the paper (Section 6). But before all that, we review existing work and recall relevant constructions ours build upon in the next section.

## 2. Related work

There are several existing techniques that locally create  $C^0$  continuous triangular patches from meshes with normals. Phong tessellation (Boubekeur and Alexa, 2008) and PN triangles (Vlachos et al., 2001) provide quadratic and cubic Bézier patches, respectively. Recently, both schemes have been generalised to arbitrary  $n$ -sided polygons by use of generalised barycentric coordinates (Hettinga and Kosinka, 2017). The patches can be constructed locally per polygon and are therefore suitable for hardware tessellation (Schäfer et al., 2014).

Locally constructing  $C^1$  patches is a well studied problem, particularly in the finite element literature. For example, Clough and Tocher (1965) create smooth piece-wise cubic interpolants over a triangulated domain based on gradients at vertices and cross-boundary derivatives at midpoints of edges. By splitting the original domain triangle into three micro-triangles,  $C^1$  continuous surfaces are constructed. Gregory (1974) modified a bi-cubic Coons patch such that derivatives at vertices can be specified without having to adhere to compatibility conditions. Mixed partial derivatives are blended by rational blending functions such that  $C^1$  continuity is achieved. However, achieving  $C^1$  continuity is not possible for arbitrary polygonal meshes due to topological constraints imposed by global parametrisations. Therefore,  $G^1$  continuity is often more appealing.

Chiyokura and Kimura (1983) created a special Bézier patch, similar to Gregory's patch, where cross-boundary tangents can be defined independently per boundary edge. Through the use of rational blending functions, edge conditions are blended smoothly so that a patch can be fitted with tangent plane continuity into an irregular quadrilateral mesh. In addition to this, a localised construction of a  $G^1$  cross-boundary tangent which can be determined from boundary curve data alone was given.

Later, Longhi (1986) used the same constructions for cubic Bézier triangles to create a triangular Gregory patch. PNG1 triangles (Fünzig et al., 2008) is a construction based on the  $C^0$  PN triangle scheme, which it augments by taking data from adjacent triangles and assuring  $G^1$  continuity for each of the adjacent triangles separately by using Farin's method (Farin, 1982). Then rational blending functions are employed to ensure that appropriate groups of control points are blended according to parametric position.

Several comparable schemes that use rational blending also exist (Boschioli et al., 2012). Shirman and Séquin (1987, 1991) construct a polynomial patch type that is highly similar to triangular Gregory patches in that  $G^1$  continuity is ensured on the boundary by the method of Chiyokura and Kimura. Instead of using rational blending functions to circumvent the twist compatibility problem, the problem is solved by employing the Clough-Tocher-Hsieh split.  $G^1$  continuity between the split triangles is then easily achieved by employing Farin's method (Farin, 1982). The structure also extends to quadrilaterals

by using a similar 4-split method, but negative results were found for  $n$ -sided surfaces. Splitting into  $n$  triangles results into incompatible conditions at the split point.

When it comes to  $n$ -sided patches, there are generally two ways of assuring smoothness with all  $n$  adjacent patches. Either the domain is filled up by separate parametric triangular or quadrilateral patches (see e.g. Malraison, 2000; Gregory et al., 1990; Karčiauskas and Peters, 2017), or a single patch is used to cover the whole domain. Our approach uses the single-patch strategy.

There exists a wealth of Gregory- and Coons-like multisided patches that use transfinite interpolation to interpolate prescribed ribbon data (Salvi and Várady, 2016; Várady et al., 2011). Similarly, in Leung et al. (2011) a localised approach leads to a multisided Gregory patch. Planar cubic Bézier boundary curves are generated and for each curve a  $G^1$  cross-boundary tangent function is determined. Using the cross-boundary tangent functions of two neighbouring edges, corner interpolators are created and  $n$  of these are blended into a final surface. The method has the downside that the input polygons should be planar or nearly planar to obtain good results. The multisided control point oriented construction of Zheng and Ball (1997) has also been extended with Gregory terms (Hall and Mullineux, 1999; Zheng, 2001) for patches with six sides or fewer. However, the parametrisation of these patches is not straightforward and no solutions exist for patches with more than six sides.

Loop and DeRose (1990) join  $S$ -patches with  $G^1$  continuity in an  $n$ -sided hole problem, but the input mesh has to adhere to certain conditions so that the twist incompatibility problem is solved. In Lodha (1993) the possibility of augmenting the  $S$ -patch structure with control points corresponding to rational blending functions is explored. An example is given for a cubic pentagonal  $S$ -patch, but it is assumed that the first two rows of control points have been prescribed, and thus a quadratic cross-boundary derivative is determined. It is noted that for each side the control points can be uniquely determined to adhere to tangent plane compatibility conditions except for pairs of control points in the corners. A more general form of multisided Bézier surfaces, where the parametrisation is not restricted to a certain type, was given in Langer et al. (2008). In addition, derivatives are provided and conditions for smooth joins between patches are discussed.

Further work has been done to create optimal layouts of generalised Bézier patches which join with  $C^0$ ,  $G^1$  and even  $G^2$  continuity using non-local methods, but again the problem is restricted to twist compatible conditions (Várady et al., 2017). One can even employ rotation minimising frames (Wang et al., 2008) to create initial  $G^1$  or  $G^2$  continuous ribbons (Salvi and Várady, 2014) from which generalised Bézier patches can be created.

For future use and to establish notation, we now provide short descriptions of the method of Chiyokura and Kimura, of triangular and quadrilateral Gregory patches, and of multisided surface representations.

### 2.1. The method of Chiyokura and Kimura

The method of Chiyokura and Kimura (1983) joins two Bézier patches smoothly by ensuring  $G^1$  continuity at shared edges by taking into account only shared positional and normal data. The method is applied to the common cubic boundary curve of two adjacent Bézier patches. Each boundary curve is defined by a control polygon, which can be used to determine positions of the inner control points of a patch.

On the common boundary  $\Gamma(u)$ ,  $u \in [0, 1]$ , of two Bézier patches  $\Phi_a(u, v)$  and  $\Phi_b(u, v)$  one can find the versal tangent vector  $\partial\Gamma(u)$  along the boundary curve and the transversal, or cross-boundary, tangent vectors  $\partial\Gamma_a(u)$  on patch  $\Phi_a(u, v)$  and  $\partial\Gamma_b(u)$  on patch  $\Phi_b(u, v)$ . A sufficient and necessary condition for  $G^1$  continuity is the co-planarity of the three tangent vectors  $\partial\Gamma(u)$ ,  $\partial\Gamma_a(u)$  and  $\partial\Gamma_b(u)$  along  $\Gamma(u)$ , i.e.,

$$\det(\partial\Gamma(u), \partial\Gamma_a(u), \partial\Gamma_b(u)) = 0, \quad u \in [0, 1].$$

This condition can be expressed in terms of scalar-valued functions  $\alpha(u)$ ,  $\beta(u)$  and  $\gamma(u)$  such that:

$$\alpha(u)\partial\Gamma(u) + \beta(u)\partial\Gamma_a(u) + \gamma(u)\partial\Gamma_b(u) = 0. \quad (1)$$

Equation (1) is used to determine control points so that a cubic patch can be joined smoothly to an auxiliary patch known as a basis patch. Consider the situation depicted in Fig. 2, where an actual patch  $\Phi_a$  is connected to a basis patch  $\Phi_b$ . Vectors  $\mathbf{c}_i$  constitute the edges of the cubic control polygon on the common boundary, and  $\mathbf{a}_i$  and  $\mathbf{b}_i$  belong to  $\Phi_a$  and  $\Phi_b$ , respectively.  $\mathbf{a}_0$  and  $\mathbf{a}_3$  are unit vectors orthogonal to  $\mathbf{c}_0$  and  $\mathbf{c}_2$ , respectively, and lie in the tangent plane of the normal defined at the vertices  $\mathbf{v}_i$  and  $\mathbf{v}_{i+1}$ , respectively. In case of the actual patch being triangular, the first row of control points from the boundary are quartic control points obtained by degree elevation. Equation (1) is then rewritten in terms of scalar functions  $k(u)$  and  $h(u)$ :

$$\partial\Gamma_a(u) = k(u)\partial\Gamma_b(u) + h(u)\partial\Gamma(u),$$

so that the actual patch is joined with  $G^1$  continuity to the basis patch. To solve this equation, first express  $\mathbf{a}_0$  and  $\mathbf{a}_3$  as

$$\mathbf{a}_0 = k_0\mathbf{b}_0 + h_0\mathbf{c}_0, \quad \mathbf{a}_3 = k_1\mathbf{b}_3 + h_1\mathbf{c}_2, \quad k_0, k_1, h_0, h_1 \in \mathbb{R},$$

and set

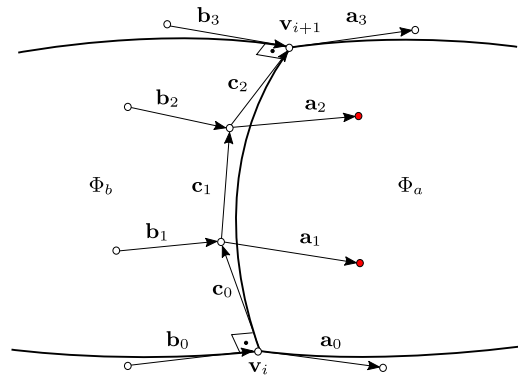


**Fig. 2.** A schematic view of the boundary conditions between the basis patch  $\Phi_b$  and the actual patch  $\Phi_a$ . The points created by the method of Chiyokura are depicted in red. (For interpretation of the colours in the figure(s), the reader is referred to the web version of this article.)

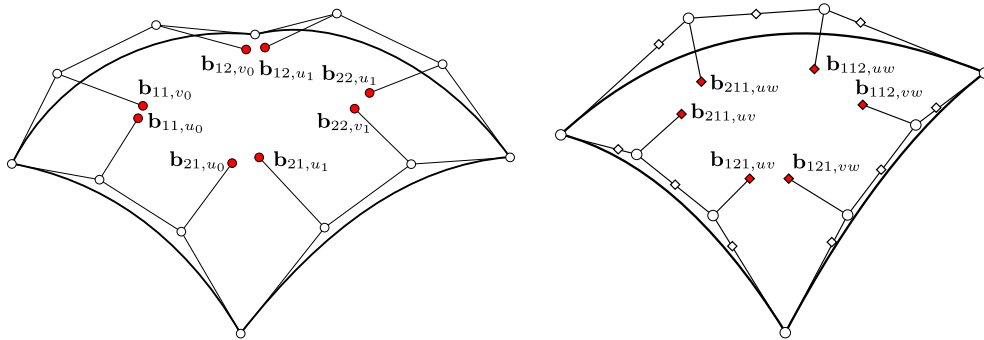


**Fig. 3.** The control net of a quadrilateral Gregory patch (left) and the control net of a triangular Gregory patch (right). The diamonds are quartic control points obtained by degree elevating cubic control points. Red points are the inner control points as constructed by the method of Chiyokura and Kimura.

$$k(u) = (1 - u)k_0 + uk_1, \quad h(u) = (1 - u)h_0 + uh_1.$$

It is then assumed that  $\partial\Gamma_b(u)$  on the basis patch is only quadratic and that vectors  $\mathbf{b}_1$  and  $\mathbf{b}_2$  can be determined by linear interpolation  $\mathbf{b}_1 = \frac{2}{3}\mathbf{b}_0 + \frac{1}{3}\mathbf{b}_3$ ,  $\mathbf{b}_2 = \frac{1}{3}\mathbf{b}_0 + \frac{2}{3}\mathbf{b}_3$ . Finally, vectors  $\mathbf{a}_1$  and  $\mathbf{a}_2$  can be determined as

$$\mathbf{a}_1 = (k_1 - k_0)\frac{\mathbf{b}_0}{3} + k_0\mathbf{b}_1 + 2h_0\frac{\mathbf{c}_1}{3} + h_1\frac{\mathbf{c}_0}{3}, \quad \mathbf{a}_2 = k_1\mathbf{b}_2 - (k_1 - k_0)\frac{\mathbf{b}_3}{3} + h_0\frac{\mathbf{c}_2}{3} + 2h_1\frac{\mathbf{c}_1}{3}.$$

The connection to a basis patch can be done without having explicit knowledge of all control points of adjacent patches; the construction relies only on data from the common boundary. The method is applied to both sides of the boundary individually such that there are two basis patches, one on either side of the boundary. The control points determined for the actual patches are positioned in such a way that the actual patches join with  $G^1$  continuity with the adjacent basis patches. The basis patches themselves join each other with  $C^1$  continuity and therefore the actual patches join each other with  $G^1$  continuity, as desired.

### 2.2. Gregory patches

The Gregory patch is a generalisation of Gregory’s ideas (Gregory, 1974) to tensor product Bézier surfaces (Chiyokura, 1986). Consider the control point layout of Fig. 3, left. The method of Chiyokura and Kimura is applied to all four boundary edges to obtain 8 inner control points (shown in red), one pair per corner. Here, the twist compatibility problem is encountered and rational blending functions are used. The functions blend the four pairs of inner control points so that they are interpolated along straight line segments. In particular,

$$\mathbf{b}_{11} = \frac{v\mathbf{b}_{11,u_0} + u\mathbf{b}_{11,v_0}}{u + v}, \quad \mathbf{b}_{21} = \frac{(1 - v)\mathbf{b}_{21,u_0} + u\mathbf{b}_{21,v_1}}{(1 - v) + u},$$

$$\mathbf{b}_{12} = \frac{v\mathbf{b}_{12,u_1} + (1 - u)\mathbf{b}_{12,v_0}}{v + (1 - u)}, \quad \mathbf{b}_{22} = \frac{(1 - v)\mathbf{b}_{11,u_0} + (1 - u)\mathbf{b}_{11,v_0}}{(1 - u) + (1 - v)}.$$

These blending functions are designed such that the blended control points are in the correct position when the patch is evaluated on an edge and thus the correct cross-boundary derivative is maintained.

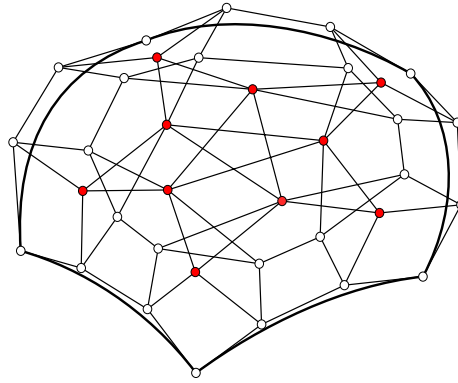


**Fig. 4.** The control point layout of a cubic pentagonal S-patch. The red control points mark the inner control points of each Bézier sub-triangle.

Longhi (1986) applies the same idea to triangular Bézier patches such that a triangular Gregory patch is constructed. Consider the layout in Fig. 3, right, of a triangle with cubic boundary curves, and the 6 points (shown in red) generated by using the method on the boundary curves after degree elevation from cubic to quartic. The degree elevation step is required to match the cubic cross-boundary derivative, corresponding to a quartic triangular Bézier patch, constructed by the method. These points describe the three inner control points of a quartic Bézier triangle. Again, pairs of these points are blended rationally:

$$\begin{aligned} \mathbf{b}_{211} &= \frac{(1-w)v\mathbf{b}_{211,uv} + (1-v)w\mathbf{b}_{211,uw}}{(1-w)v + (1-v)w}, \\ \mathbf{b}_{121} &= \frac{(1-w)u\mathbf{b}_{121,uv} + (1-u)w\mathbf{b}_{121,vw}}{(1-w)u + (1-u)w}, \\ \mathbf{b}_{112} &= \frac{(1-u)v\mathbf{b}_{112,vw} + (1-v)u\mathbf{b}_{112,uw}}{(1-u)v + (1-v)u}. \end{aligned}$$

Both techniques contain simple singularities in the parametrisation at the vertices, but they can easily be handled by analysing the parameter values.

2.3. Multisided surface representations

Bézier triangles is a successful technique to define surfaces over triangular regions by using barycentric coordinates. Likewise, tensor product Bézier surfaces possess equal qualities, but are defined over quadrilateral regions and use bi-linear coordinates. However, when dealing with regions with more than four sides the parametrisation should be done using generalised barycentric coordinates.

Generalised barycentric coordinates provide a coordinate system in which any point  $\mathbf{p}$  on a planar polygon can be expressed as a weighted combination of the polygon’s vertices. Given a cyclic ordering of vertices  $\mathbf{v}_i, i = 1 \dots n$  of a polygon, barycentric coordinate functions  $\phi_i, i = 1 \dots n$  partition unity  $\sum_{i=1}^n \phi_i = 1$ , are non-negative  $\phi_i \geq 0, \forall i$  on the polygon, and satisfy the barycentric property  $\sum_{i=1}^n \phi_i(\mathbf{p})\mathbf{v}_i = \mathbf{p}$ . The coordinate functions linearly interpolate on the boundary, and satisfy the Lagrange property  $\phi_i(\mathbf{v}_j) = \delta_{ij}$ , where  $\delta_{ij}$  is the Kronecker delta. When  $n = 3$  the coordinates are the same as the regular barycentric coordinates. For  $n > 3$  the coordinates are no longer unique. An extensive overview of generalised barycentric coordinates can be found in Floater (2015). To parametrise an arbitrary non-planar polygon, we use an auxiliary parametrisation domain, a regular polygon of valency  $n$ , which is parametrised by Wachspress coordinates (Wachspress, 1975; Hettinga and Kosinka, 2017).

Bézier surfaces that use generalised barycentric coordinates are referred to as multisided Bézier surfaces or S-patches (Loop and DeRose, 1989). An S-patch has the following definition:

$$\mathbf{p}_n^d(\phi) = \sum_{|\alpha|=d} \mathbf{b}_\alpha B_\alpha^d(\phi) \quad \text{with} \quad B_\alpha^d(\phi) = \frac{d!}{\alpha!} \phi_\alpha. \tag{2}$$

Here,  $d$  is the degree of the surface,  $n$  is the number of sides,  $\mathbf{b}_\alpha$  are the control points, and  $B_\alpha^d(\phi)$  are the multinomial expansions of the Bernstein polynomials using generalised barycentric coordinates  $\phi = (\phi_1, \dots, \phi_n)$  with  $\alpha = (\alpha_1, \dots, \alpha_n) \in \mathbb{N}^n, \alpha! = \prod_i \alpha_i$  and  $\phi_\alpha = \prod_i \phi_i^{\alpha_i}$ .

When  $n = 3$ , the coordinates  $\phi$  are just the regular barycentric coordinates, and thus Bézier triangles are reproduced. When  $n = 4$  and  $\phi$  are the Wachspress coordinates (Wachspress, 1975) on a square domain, it can be easily seen that the S-patch becomes a tensor product Bézier surface since the coordinate functions reduce to bilinear coordinates. All these nice

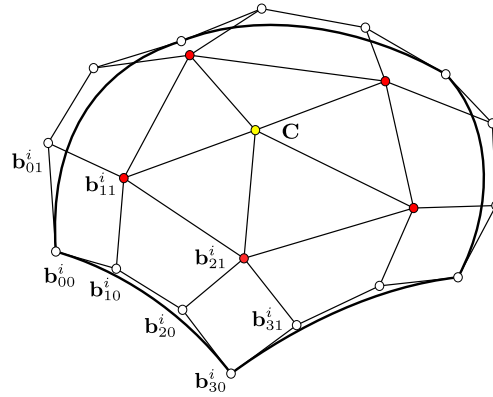


**Fig. 5.** The control net of a cubic generalised Bézier patch. The centre control point is depicted in yellow and internal control points in red. The labelling of the control points corresponding to one side is given, the rest can be labelled analogously.

properties make S-patches an attractive choice for geometric modelling. However, the control point structure increases in complexity as the number of sides increases and also when the degree of the patch increases. It can be quite challenging to manually or even automatically position all the control points to get a desired surface.

Intuitively, when  $d = 2$  or  $d = 3$ , S-patches can be interpreted as a combination of all possible degree  $d$  triangular Bézier patches that can be constructed from all unique triangles on a polygonal domain. For a polygon with  $n$  sides, there are  $\binom{n}{3}$  unique triangles that can be constructed. For  $n = 5$ , there are already 10 such triangles. In our cubic example in Fig. 4, the centre control point of each such triangle is marked in red.

Generalised Bézier patches (Várady et al., 2016), or GB patches, are a multisided control structure that combines transfinite and control-point-oriented structures. Like for S-patches, generalised barycentric coordinates are used to define local parameters and blending functions. The resulting patches and structure are loosely similar to tensor product Bézier surfaces and they inherit many of their properties.

A GB patch is a combination of  $n$  Bézier ribbons. On each side of the patch a degree  $d$  Bézier ribbon is defined by taking into account  $l$  rows of  $d + 1$  control points with  $l = (d + 1) \bmod 2$ . For each ribbon, bivariate tensor-product Bernstein polynomials are used:

$$\mathbf{S}_i^d(s_i, h_i) = \sum_{j=0}^d \sum_{k=0}^l \mu_{jk}^i \mathbf{b}_{jk}^i B_{jk}^d(s_i) B_{jk}^d(h_i).$$

For ribbon  $i$  of a patch, which corresponds to the edge spanned from vertex  $\mathbf{v}_{i-1}$  to  $\mathbf{v}_i$ , local parameter functions can be defined using generalised barycentric coordinates  $\phi$ :

$$s_i = \frac{\phi_i}{\phi_i + \phi_{i-1}}, \quad h_i = 1 - \phi_i - \phi_{i-1},$$

where  $s_i$  is known as the side parameter and  $h_i$  as the distance parameter. They are constructed so that they have the same behaviour as ordinary bilinear coordinates.  $s_i$  varies from 0 to 1 on side  $i$ , and  $h_i$  is 0 exactly on side  $i$  but increases on the interior of a patch and linearly on sides  $i + 1$  and  $i - 1$ .  $\mathbf{b}_{jk}^i$  are the control points as oriented from side  $i$ . The labelling of control points of a single ribbon is given in Fig. 5. The control points of the remaining sides are labelled analogously and control points in the corners are shared between ribbons.  $\mu_{jk}^i$  is a scalar function that serves the purpose of assuring locality of the influence of each side, as well as blending control points which are shared by multiple sides such that they are weighted by a linear combination of Bernstein polynomials. It is defined for  $d \leq 3$  as

$$\mu_{jk}^i = \begin{cases} \frac{h_{i-1}}{h_i + h_{i-1}} & j < 2 \\ 1 & 2 \leq j \leq d - 1 \\ \frac{h_{i+1}}{h_i + h_{i+1}} & j > d - 1 \end{cases} \quad (3)$$

For higher degrees, these functions have to deal with certain other constraints (Várady et al., 2016), but these do not concern us as we are interested only in the cubic case.

Adding all contributions results in a patch definition that is not necessarily affine invariant, meaning that the weighted Bernstein polynomials of all the sides may not sum to unity. This can be easily fixed by augmenting the patch structure with another central control point  $\mathbf{C}$  and its associated blending function



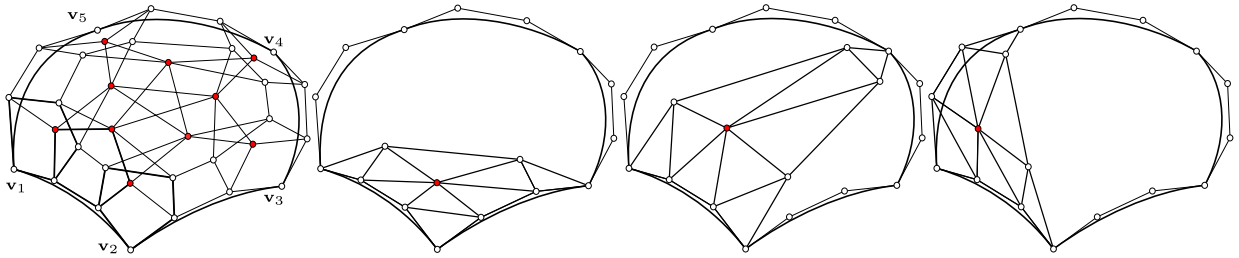


**Fig. 6.** A pentagonal cubic S-patch. The three boundary panels in bold on the far left can be seen as coming from three distinct Bézier sub-triangles (left to far right):  $T(\mathbf{v}_1, \mathbf{v}_2, \mathbf{v}_3)$ ,  $T(\mathbf{v}_1, \mathbf{v}_2, \mathbf{v}_4)$ , and  $T(\mathbf{v}_1, \mathbf{v}_2, \mathbf{v}_5)$ .

$$B_0^d = 1 - \sum_{i=1}^n \sum_{k=1}^l \sum_{j=0}^d \mu_{jk}^i B_{jk}^d(s_i) B_{jk}^d(h_i).$$

This function employs the principle of weight deficiency, which is a versatile correction term. It adds the weight that is needed to have functions exactly partition unity, by adding that which is deficient and assigning this to some centrally placed control point. This centre point is best placed somewhere in the inner-most ring of control points of the patch. It is assumed that the ribbons on each side provide  $G^1$  continuity with respect to adjacent patches and are internally twist compatible. Combining all these elements yields the following definition of a GB patch:

$$\sum_{i=1}^n \mathbf{S}_i^d(s_i, h_i) + B_0^d \mathbf{C}.$$

We are now ready to introduce our first construction of multisided patches with  $G^1$  continuity between adjoining patches.

### 3. Gregory S-patches

General conditions for a  $G^1$  join between S-patches are given in Loop and DeRose (1990). The conditions can be interpreted in two ways. First, they can be viewed in terms of boundary panels. Each boundary panel is a group of  $n$  control points oriented in a ring-like structure. Three of these panels are highlighted as bold pentagons in Fig. 6, far left. A way to join S-patches smoothly is to make sure that the boundary panels are affine images of each other and that the panels are co-planar with the panels of the adjoining patch (Farin, 1986). However, this procedure is difficult and requires that many control points have to be in more than one position as the conditions for adjacent boundaries might not be compatible, similar to the conditions of PNG1 triangles (Fünfzig et al., 2008).

Secondly, the  $G^1$  conditions can be interpreted in terms of Bézier sub-triangles. As mentioned in Section 2.3, S-patches can be seen as combinations of unique triangular Bézier patches that can be constructed on an  $n$ -sided polygon. Using this property, the control points of the boundary panels can be decomposed into control points of Bézier sub-triangles. This is illustrated in Fig. 6, left to far right. Smoothly joining these Bézier sub-triangles to an adjoining patch is subject to the general conditions for a  $G^1$  join between triangular Bézier patches. For a polygon with  $n$  sides there are  $n - 2$  Bézier sub-triangles per edge which determine the conditions for  $G^1$  continuity across that edge, and each of these should be joined smoothly to an adjoining patch. This in turn means that all the boundary panels have been set and the S-patch will join with  $G^1$  continuity to the adjacent patch.

Each Bézier sub-triangle  $T(\mathbf{v}_{i-1}, \mathbf{v}_i, \mathbf{v}_j)$  on side  $i$  (the edge given by  $\mathbf{v}_{i-1}$  and  $\mathbf{v}_i$ ) has the cross-boundary derivative  $\partial T(\mathbf{v}_{i-1}, \mathbf{v}_i, \mathbf{v}_j)(u)$  on the edge  $\Gamma_i(u)$  with  $u \in [0, 1]$ . Here, the cross-boundary derivative is taken in some arbitrary parametric direction not along  $u$ . As shown e.g. by Farin (1982), the derivative of a degree-elevated triangular Bézier patch can be expressed in terms of the ‘elevated’ control points in the first row in from the edge and the original control points on the boundary edge. This also applies to the sub-triangles.

Turning back to Equation (1), we obtain for each sub-triangle on side  $i$  that

$$\alpha_{i,j}(u) \partial \Gamma_i(u) + \beta_{i,j}(u) \partial T(\mathbf{v}_{i-1}, \mathbf{v}_i, \mathbf{v}_j)(u) + \gamma_{i,j}(u) \partial \Gamma_b(u) = 0,$$

where  $\partial \Gamma_b(u)$  is the cross-boundary derivative of the adjoining patch at side  $i$ . And we know from Section 2.1 that this can be solved using the method of Chiyokura and Kimura, applied to each sub-triangle separately, including rational blending of some of the arising control points. This then implies that all the sub-triangles will connect with  $G^1$  continuity to the adjoining patch, which in turn means that the constructed Gregory S-patch, which is a combination of its sub-triangles, will be  $G^1$ -connected as well.

The case of four sided polygons is examined first.



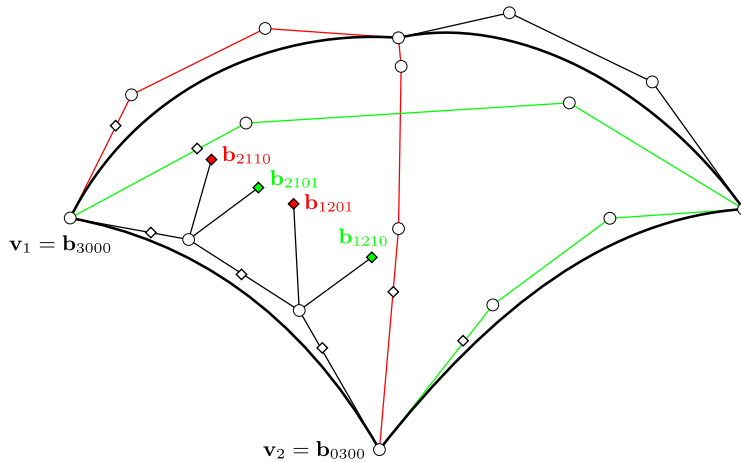


**Fig. 7.** A schematic view of the first row of control points of a quadrilateral cubic (Gregory) S-patch from one side. The points denoted by diamonds are degree elevated cubic control points. The two Bézier sub-triangles are denoted in red and green as well as the inner control points obtained by using the method of Chiyokura and Kimura for both sub-triangles. The rest of the control points have been omitted.

### 3.1. Quadrilateral Gregory S-patches

The quadrilateral Gregory S-patch builds on the quadrilateral cubic S-patch where all edge control points have been determined. These control points are shown as white bullets in Fig. 7. This includes the control points of internal edges, e.g. the edge spanned from vertex  $\mathbf{v}_i$  to  $\mathbf{v}_{i+2}$ . Edges like these are not edges in the traditional sense, but can be interpreted as edges of Bézier sub-triangles. In our construction, we set all these control points by projecting points on the edges of the input polygon onto tangent planes of the normals defined at vertices, as proposed in Hettinga and Kosinka (2017), Vlachos et al. (2001).

As mentioned above, the conditions on the boundary are determined by a select few of the Bézier sub-triangles. In the case of quadrilaterals these are only two per boundary, pictured as the red and the green triangle in Fig. 7. Chiyokura and Kimura’s method is applied to both of these triangles after all edge curves, including edges spanned over the interior of the polygon, have been degree elevated to quartic curves. Only the pairs of points generated at corners have to be blended rationally.

The blending functions are a straightforward generalisation from the triangular case of Gregory patches, and are best understood as being oriented from a corner. The blending function of the  $i$ -th corner for two control points  $\mathbf{p}_{i-1}$  and  $\mathbf{p}_{i+1}$  is:

$$\beta_i(\mathbf{p}_{i-1}, \mathbf{p}_{i+1}) = \frac{(1 - \phi_{i+1})\phi_{i-1}\mathbf{p}_{i-1} + (1 - \phi_{i-1})\phi_{i+1}\mathbf{p}_{i+1}}{(1 - \phi_{i+1})\phi_{i-1} + (1 - \phi_{i-1})\phi_{i+1}}. \tag{4}$$

This ensures that on the side of vertices  $\mathbf{v}_{i-1}$  and  $\mathbf{v}_i$  the blending function results in point  $\mathbf{p}_{i-1}$ , and on the side of vertices  $\mathbf{v}_i$  and  $\mathbf{v}_{i+1}$  the blending function yields point  $\mathbf{p}_{i+1}$ . In total there are thus 4 such blending functions, one for each corner. It is easy to see that when  $n = 3$  the blending functions of Longhi (1986) are reproduced.

As stated before, the rest of the control points generated by the method of Chiyokura and Kimura can be used without blending and are quartic control points. Therefore, all remaining cubic control points should be degree elevated to quartic such that the end result is a quartic S-patch with four rationally blended inner control points. In addition to this, another control point results from degree elevating the S-patch. This control point can be regarded as another type of centre control point and its associated Bernstein control function is  $B_{1111}^4(\phi)$ . It should be noted that this centre control point does not affect the derivatives on the boundaries. This type of control point only occurs in patches with more than 3 sides, and thus Gregory S-patches exactly reproduce triangular Gregory patches. The resulting surfaces for the quadrilateral case are slightly different from quadrilateral Gregory patches due to the extra control point and the difference in degree.

### 3.2. Generalisation to arbitrary polygons

Now that the basic foundation has been made, the step towards arbitrary polygons is taken easily. Again, a net of cubic boundary curves is generated. Then all boundary curves are degree-elevated to quartics and the method of Chiyokura and Kimura is applied to all relevant Bézier sub-triangles (those that contain a boundary edge). Control points in the corner of the patches will have double definitions relative to which side they have been constructed from. These points are blended using the generalised rational blending functions of Equation (4).

For  $n > 3$ , this will not set the positions for all inner control points. A few inner points are free to set Loop and DeRose (1990) as they have no effect on the boundary. The number of free control points is given by  $3\binom{n}{3} - 2n(n - 2) + n + \binom{n}{4}$ . This

**Table 1**

A table showing the number of inner control points and how many of those are free to set per valency.

Valency	3	4	5	6	7	8
all	12	31	65	120	203	322
inner	3	13	35	75	140	238
free	0	1	10	33	77	150

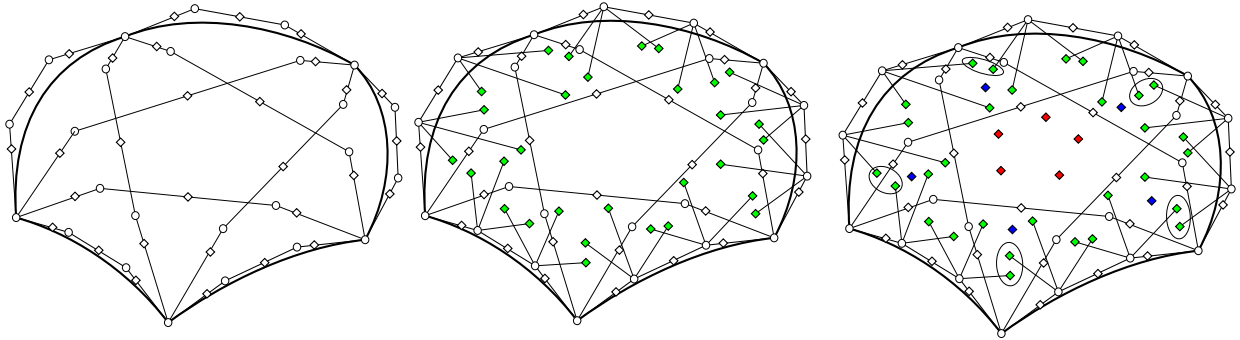


**Fig. 8.** A schematic view of the steps involved in constructing a Gregory S-patch. From left to right: Construction of edge curves and degree-elevation of edge curves, application of the method of Chiyokura and Kimura to boundary curves, and setting the positions of the free control points. White bullets represent cubic control points, white diamonds represent quartic control points for edge curves, green diamonds represent points constructed by the method of Chiyokura and Kimura, blue diamonds are free quartic Bézier sub-triangle points, and red are free quartic centre points.

can be determined by seeing that there are  $\binom{n}{3}$  sub-triangles which have 3 inner control points each. The method constructs two points for each  $(n-2)$  of these sub-triangles on each edge. Then there are still  $n$  points too many as there are duplicate control points at each corner. Lastly, the addition of quartic centre control points adds another  $\binom{n}{4}$  free control points. The number of free control points, which grows quartically with  $n$ , is shown in Table 1. The total number of control points is  $3\left(\binom{n}{2} + \binom{n}{3}\right) + \binom{n}{4}$ .

The construction of a Gregory S-patch can be summarised in the following steps:

- Construct cubic Bézier edge curves by projecting points onto the tangent planes defined at the vertices (see Hettinga and Kosinka, 2017; Vlachos et al., 2001).
- Degree-elevate all constructed curves to quartic Bézier curves.
- Identify for each boundary edge the  $n-2$  connected incomplete Bézier sub-triangles, then
  - Use Chiyokura and Kimura’s method (see Section 2.1) to construct two inner control points (depicted as green diamonds in Fig. 8) per Bézier sub-triangle using the data of the boundary curve and the adjacent quartic Bézier curves that form the incomplete Bézier sub-triangle.
  - Construct a rationally blended control point by combining duplicate control points (encircled by ellipses in Fig. 8, right), one per pair, in the corners of the patch with the rational blending functions of Equation (4).
- For all incomplete Bézier sub-triangles
  - Calculate positions for the free control point(s) (depicted as blue diamonds in Fig. 8, right) by averaging positions of previously determined inner control points of other Bézier sub-triangles.
- Construct positions of quartic centre points (depicted as red diamonds in Fig. 8, right) by averaging control point positions of previously determined inner control points.

Our Gregory S-patch differs from the S-patch with Gregory terms described by Lodha (1993), where the involved derivatives are quadratic, whereas our derivatives are cubic. Constructing a quadratic derivative locally requires that one or more scalar functions in Equation (1) have to be fixed or that many control points need double definitions. This restricts the freedom in setting the boundary curves and makes it difficult or even impossible to construct cross-boundary derivatives locally.

The large number of free control points can be used as shape handles to control the shape of the interior of the patch. However, currently we set the positions of these control points as convex combinations of other control points. Another good heuristic might be to ensure cubic precision, but visually this might barely affect the resulting surface as the influence of the free control points is typically minimal, especially for lower valencies.

Since many of the control points of the Gregory S-patches are free to set, they can also be replaced by a single control point by employing the same principle of weight deficiency, as for GB patches, into the S-patch structure. By evaluating only the basis functions of control points that are determined by  $G^1$  continuity, the deficient weight can be efficiently determined. This can be done by summing all relevant basis functions and subtracting this from unity. This deficient weight can then be assigned to a centrally placed control point.

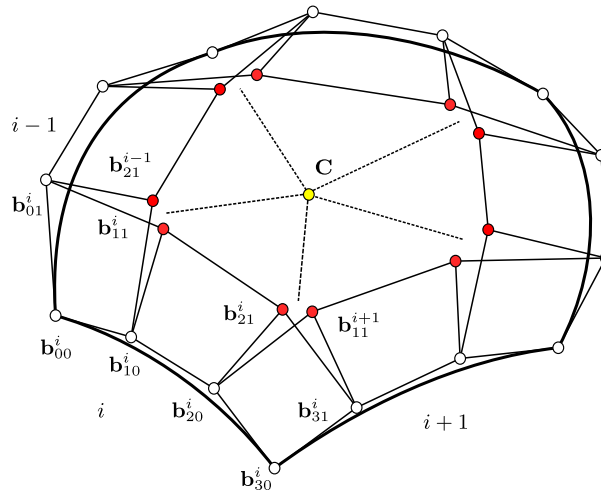


Fig. 9. The control net of a pentagonal Gregory GB patch. Red points are points constructed by Chiyokura and Kimura’s method and the centre control point is marked in yellow.

#### 4. Gregory generalised Bézier patches

The default form of generalised Bézier (GB) patches, as given in Várady et al. (2016), assumes that the twist compatibility problem has been solved. In this way, adjacent ribbons can be matched inside a GB patch such that the ribbons connect with  $G^1$  continuity to adjacent patches and also are internally compatible by sharing certain control points. However, solving twist conditions for arbitrary meshes can be an expensive pre-processing step (Salvi and Várady, 2014). We now show that the same method of locally creating independent  $G^1$  joins per edge can be applied to GB patches.

Consider an  $n$ -sided polygon with normals defined at vertices. For each edge two extra control points can be defined by using projections onto tangent planes such that a loop of cubic Bézier boundary curves is created, again following the approach taken for curved PN triangles (Vlachos et al., 2001). The boundary control points are marked by white bullets in Fig. 9. The method of Chiyokura and Kimura can be applied again, yielding, like with Gregory patches and Gregory S-patches, doubly defined control points at each corner, which have to be dealt with appropriately. The construction of a Gregory GB patch is a simple process and can be summarised in the following way:

- Construct cubic Bézier boundary edge curves by projecting points onto the tangent planes defined at the vertices (see Hettinga and Kosinka, 2017; Vlachos et al., 2001).
- For each boundary curve use Chiyokura and Kimura’s method (see Section 2.1) to construct two inner control points (depicted as red bullets in Fig. 9).
- Construct the centre control point by averaging inner control points (depicted as a yellow bullet in Fig. 9).

Due to the structure of GB patches, the blending of these control points does not have to be done explicitly. Instead, it can be achieved by slightly changing the structure of the patch so that certain control points are not shared between ribbons. The control structure of Gregory GB patches can be seen in Fig. 9. The control points in the corners of an ordinary GB patch (see Fig. 5) have now been split into two points each such that they adhere to the  $G^1$  conditions of their respective boundary edges. The evaluation of each ribbon is then done using only its corresponding control points. No explicit blending similar to Equation (4) is applied to the corner control points as the scalar functions  $\mu_{jk}^i$  (see Equation (3)) can be used to do just this. It also means that no degree-elevation is needed.

If the twist terms of adjacent ribbons coincide, the standard form of the GB patch is reproduced. The quadrilateral form of a Gregory patch is reproduced as we use a square parameter domain in combination with Wachspress, and thus bilinear, coordinates. No weight deficiency occurs in this case.

##### 4.1. $G^1$ continuity

It remains to show that the adjusted layout of control points guarantees that the patches behave like normal Bézier patches on patch boundaries and that they can be joined smoothly to other patches. As demonstrated in Várady et al. (2016), the cross-boundary derivative  $\partial\Gamma_i(u)$  of a GB patch along the  $i$ -th edge is solely determined by the first two rows of control points, namely

$$\partial\Gamma_i(s_i) = 3 \sum_{j=0}^3 (\mathbf{b}_{j1}^i - \mathbf{b}_{j0}^i) B_j^3(s_i). \tag{5}$$

Moreover, the ribbons of the distant sides have no effect on the boundary conditions (Section 2.3). In addition, Bernstein functions are reproduced on  $\Gamma_i(s_i)$ .

Since the only difference from the original GB patches are the extra control points in each corner instead of control points which are shared between ribbons, it suffices to address only the corresponding blending functions. For example, in the original GB patch  $\mathbf{b}_{21}^{i-1} = \mathbf{b}_{11}^i$  and this control point's blending function is

$$\mu_{21}^{i-1} B_{21}^3(s_{i-1}, h_{i-1}) + \mu_{11}^i B_{11}^3(s_i, h_i).$$

In contrast, the two control points don't have to coincide in the generalised construction, and  $\mathbf{b}_{21}^{i-1}$  corresponds to  $\mu_{21}^{i-1} B_{21}^3(s_{i-1}, h_{i-1})$  and  $\mathbf{b}_{11}^i$  to  $\mu_{11}^i B_{11}^3(s_i, h_i)$ .

The influence of the control points belonging to the edges adjacent to  $\Gamma_i(s_i)$  vanishes since  $\mu_{21}^{i-1} = 0$  and  $\mu_{11}^i = 1$ . This also happens in the new control structure. In the left corner with respect to  $\Gamma_i$ , see Fig. 9, we have  $\mathbf{b}_{21}^{i-1}$  with  $\mu_{21}^{i-1} B_{21}^3(s_{i-1}, h_{i-1})$ , where  $\mu_{21}^{i-1} = \frac{h_i}{h_i + h_{i-1}}$  (see Equation (3)). It is clear that  $\mu_{21}^{i-1} = 0$  on side  $i$  since  $h_i = 0$ . The same argument applies to the right corner as well.

It remains to treat derivatives. Again, the cross-boundary derivative is taken in some arbitrary parametric direction not along  $s_i$ . The contribution of the derivative of side  $i$  on  $\Gamma_{i+1}$  for  $j > d - 2$ , is (Várady et al., 2016):

$$\partial \left( \frac{h_{i+1}}{h_i + h_{i+1}} B_{j,k}^3(s_i, h_i) \right) \Big|_{\Gamma_{i+1}} = \frac{\partial(h_{i+1})}{h_i} B_{j,k}^3(s_i, h_i) \Big|_{\Gamma_{i+1}}. \quad (6)$$

On  $\Gamma_i$  with respect to the left corner we obtain

$$\partial \left( \frac{h_{i-1}}{h_i + h_{i-1}} B_{j,k}^3(s_i, h_i) \right) \Big|_{\Gamma_i} = \partial B_{j,k}^3(s_i, h_i) - \frac{\partial(h_i)}{h_{i-1}} B_{j,k}^3(s_i, h_i) \Big|_{\Gamma_i}. \quad (7)$$

In the original setting the second term either vanishes as  $h_i = 0$ , or is cancelled out by the contribution from side  $i - 1$  with respect to  $h_i$  on  $\Gamma_i$

$$\frac{\partial(h_i)}{h_{i-1}} B_{d,j}^3(s_{i-1}, h_{i-1}) \Big|_{\Gamma_i} = \frac{\partial(h_i)}{h_{i-1}} B_{j,0}^3(s_i, h_i) \Big|_{\Gamma_i}, \quad j < 2.$$

This last part can be seen from Equation (6) by switching around the indices such that it becomes the contribution of side  $i - 1$  with respect to side  $i$ . In addition,  $h_i = 1 - s_{i-1} = 0$  and  $s_i = h_{i-1}$  on  $\Gamma_i$  (Várady et al., 2016).

For  $j = 1$  and  $k = 1$  in the Gregory GB patch case, the second term in Equation (7) is not cancelled out as the blending functions don't share the same control point, and we get

$$\left( \partial(B_{1,1}^3(s_i, h_i)) - \frac{\partial(h_i)}{h_{i-1}} B_{1,1}^3(s_i, h_i) \right) \Big|_{\Gamma_i} \mathbf{b}_{11}^i + \left( \frac{\partial(h_i)}{h_{i-1}} B_{1,1}^3(s_i, h_i) \right) \Big|_{\Gamma_i} \mathbf{b}_{21}^{i-1}.$$

However, since the derivative is evaluated on  $\Gamma_i$  we have  $h_i = 0$ . This means that Bernstein polynomials for the offending terms vanish,  $B_{1,1}^3(s_i, h_i) = B_{1,1}^3(s_i, 0) = 0$ , and the original derivative  $\partial(B_{1,1}^3(s_i, h_i))$  is retained, as we set out to show.

The addition of the extra control points makes it so that each ribbon can express cross-boundary derivatives independently. By using the same structure of blending functions, twist compatibility constraints are resolved as the mixed derivatives are blended similarly as in ordinary Gregory patches.

It is clear that the structure is suitable for a very compact way of creating  $G^1$  multisided patches locally per polygon. The patches offer a much simpler structure than Gregory S-patches, which have a relatively high number of control points in comparison. Moreover, the Gregory GB patch remains cubic and need not be degree elevated to quartic, to suit the inner control points. Consequently, the total number of control points of a Gregory GB patch is  $5n + 1$ , and thus grows only linearly with  $n$ , instead of quartically. This fact can easily be seen from the control point structure of a Gregory S-patch (see Fig. 8) compared to the structure of a Gregory GB patch (see Fig. 9).

## 5. Results & discussion

We now present and discuss results obtained with the two methods. For all meshes shown in this section, vertex normals have been obtained by averaging face normals. The normals along with the vertices of a single polygon are used as an input to generate Gregory S-patches and Gregory GB patches. As mentioned above, boundary control points are set using the projection method of curved PN triangles and all parametrisations are done using Wachspress coordinates over regular polygons.

The triangular case of Gregory GB patches is interesting as the control point layout is very similar to triangular Gregory patches. As both constructions involve the use of the same methods for satisfying the boundary conditions the resulting surfaces are nearly identical. Even though triangular Gregory (S-)patches use degree elevated boundary curves, the results are still very similar as can be seen in Fig. 10.

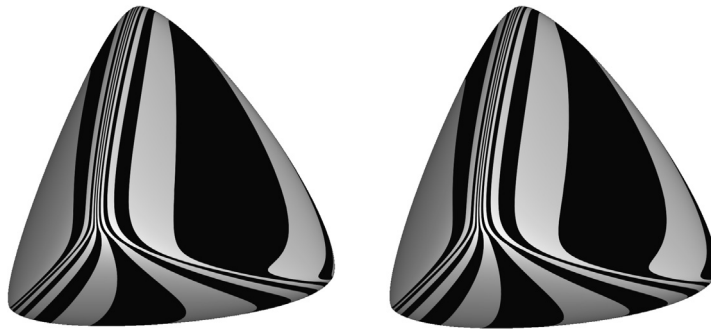


**Fig. 10.** Reflection lines on a tetrahedron model with triangular Gregory (S-)patches (left) and triangular Gregory GB patches (right).

The results of applying Gregory S-patches and Gregory GB patches to simple shapes are shown in Fig. 11. The methods are able to join together patches with any number of sides, as well as faces which are non-convex and highly irregular as can be seen in Fig. 12; see also the accompanying video material. In some cases, non-convex polygons will give undesirable results, in particular when the polygonal domain is planar or nearly planar. In this case the re-entrant corners will fold over and create sharp creases, as is the case with the original S-patch method and nearly all multisided patch schemes.

The techniques differ from other locally constructed Gregory-like patches (Leung et al., 2011) that use transfinite interpolation to interpolate boundary conditions smoothly on the interior of a patch, as Gregory S-patches and Gregory GB patches are entirely determined by control points. In addition, the construction of the cross-boundary tangent is not exclusive to the techniques and does not depend on the actual polygonal domain, making it possible to support arbitrary domains by using an auxiliary regular parametrisation domain (Hettinga and Kosinka, 2017) and to embed arbitrary ribbon data.

The resulting surfaces for Gregory GB patches seem to be very similar to Gregory S-patches. This is due to the same way of solving the  $G^1$  conditions on the edges. Differences in fullness can be attributed to the placement of the centre control point and the placement of free control points of Gregory S-patches. It has been noted that influence of the centre control point increases when a polygon with a greater number of sides is considered for GB patches (Várady et al., 2017).

Gregory S-patches and GB patches can be smoothly joined together as can be seen in Fig. 13. In this way, all types of Gregory patches can be used on a polygonal mesh.

The free control points and the normals can be perceived as the shape handles of the surface patches. Generally, the method of Chiyokura and Kimura generates visually pleasing joins between patches, but the normals at vertices should not have too great a difference with the actual surface normal of the input face. In such extreme cases the surface might bend and create bumps and cusps at boundaries so as to meet the boundary conditions. It has been noted before (Chiyokura, 1986) that the extremely localised approach might create unsatisfactory results if not applied to ‘reasonable’ meshes. Alternatively, the visual connection between patches can be improved by taking into account information about adjacent patches. Naturally, the ribbon data can be supplied without using localised methods to determine control points. The structure of the patches is not exclusive to the method of Chiyokura and Kimura and ribbon data can be embedded into Gregory S-patches and Gregory GB patches as well.

The use of the method of Chiyokura and Kimura to construct ribbons for GB patches provides a compact and local method to construct  $G^1$  multisided patches. In contrast to the proposed methods in Várady et al. (2016, 2017), this method is completely local, requiring only vertices and normals per polygon, and therefore suitable for GPU tessellation. This also applies to Gregory S-patches as these too can be generated entirely on the GPU. The use of an auxiliary regular parametrisation domain has no unwanted effects on the resulting surfaces.

The sum of the basis functions of cubic (Gregory) GB patches are plotted in Fig. 14 on the regular parametrisation domains. As noted in Várady et al. (2016), weight excess occurs in the triangular case but stays below 1.15. As mentioned before, the square domain exhibits no weight deficiency and the basis functions sum to unity. Weight deficiency occurs only in polygons with more than four sides.

Our implementation uses OpenGL tessellation shaders to render the multisided patches sending only the required data, vertices and normals, to the GPU. With regard to performance, Gregory S-patches perform worse than Gregory GB patches due to the high number of control points, especially if the mesh contains faces of high valency.

## 6. Conclusion

The use of Chiyokura and Kimura’s method in multisided control structures such as S-patches and generalised Bézier patches provides a basis for the generalisation of triangular and quadrilateral Gregory patches to arbitrary polygons. The local nature of the method is easily extended to multisided faces. A reformulation for the conditions of  $G^1$  continuity for S-patches creates an opportunity to generalise the method of Chiyokura and Kimura to such structures. In addition, the generalisation of the rational blending functions using generalised barycentric coordinates solves the twist compatibility problem. Thus, S-patches can be fit with  $G^1$  continuity into an irregular mesh of Gregory patches. However, a general



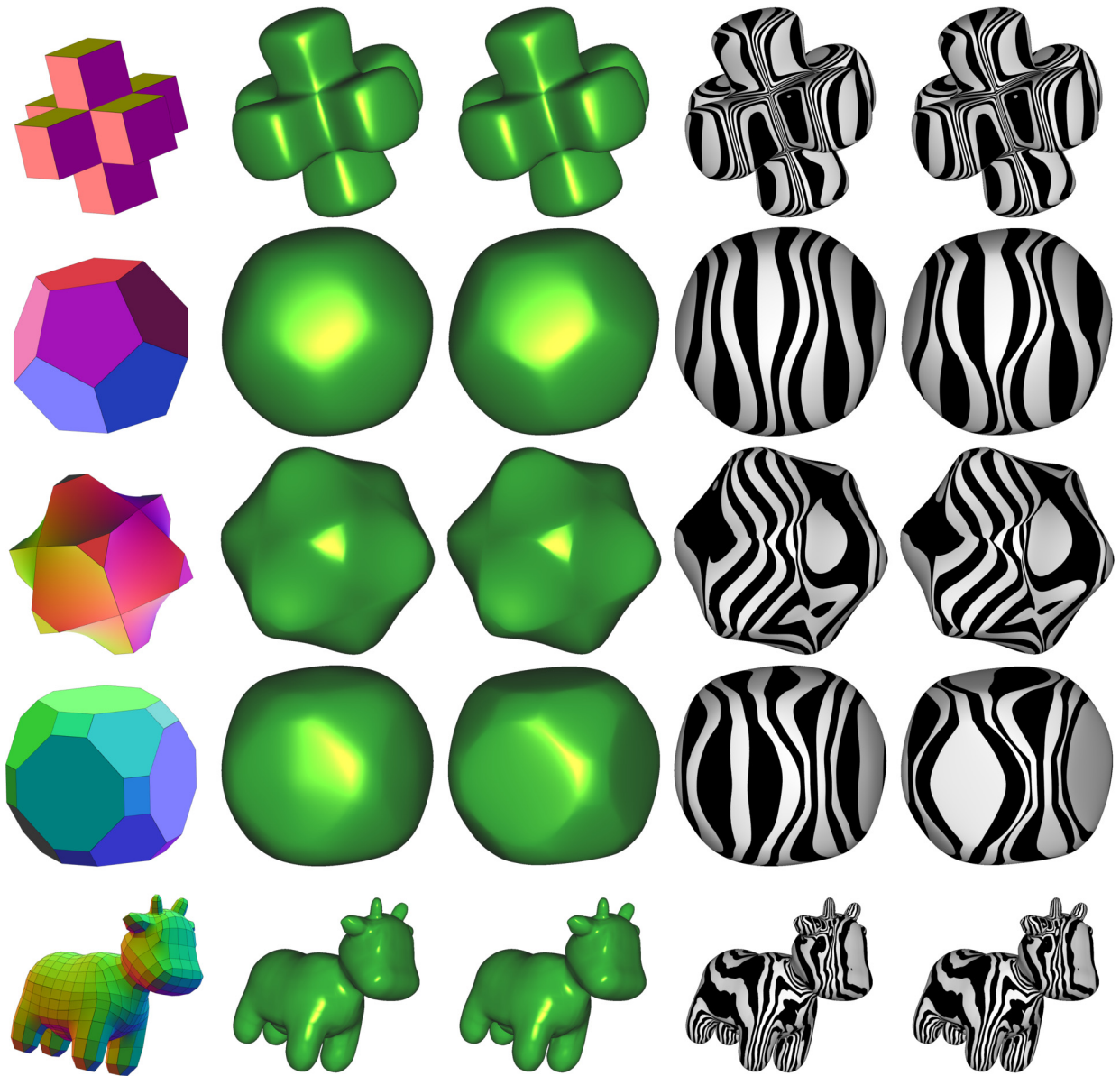


**Fig. 11.** From left to right: The input mesh (normal maps), shading on Gregory S-patches, shading on Gregory GB patches, reflection lines on Gregory S-patches, and reflection lines on Gregory GB patches. Polygons of the input meshes from top to bottom: 30 quads (3D cross); 12 pentagons (dodecahedron); 8 triangles, 12 hexagons; 8 quads 8 hexagons and 6 octagons; 56 triangles, 634 quads, 40 pentagons and 4 hexagons (Spot).

problem with the S-patch structures persists, namely the large number of control points. This can be partly solved by introducing weight deficiency into (Gregory) S-patches.

Generalised Gregory Bézier patches have fewer control points compared to S-patches and generate similar surfaces. The augmentation of the original structure with just a few extra control points creates ribbons that can define cross-boundary derivatives independently per side. The original blending functions have the inherent ability to blend boundary conditions much like the rational blending functions of Gregory patches.

The ability of local methods to construct  $G^1$  continuous joins between multisided patches make them very suitable tools in geometric modelling and computer graphics, as they provide pleasing visual results. Moreover, the localised construction makes them suitable for use on polygonal meshes such that they can be rendered efficiently using hardware tessellation (Hettinga et al., 2018).

### Acknowledgements

This paper is in part based on the first author's MSc thesis at the University of Groningen.

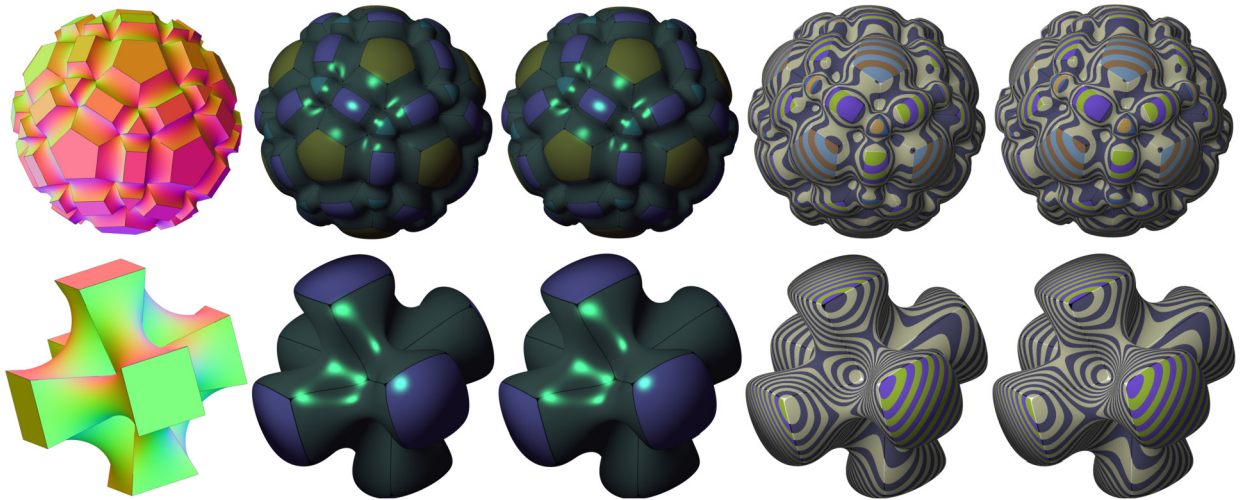


**Fig. 12.** From left to right: the input mesh (normal maps), shading on Gregory S-patches, shading on Gregory GB patches, planar slicing on Gregory S-patches, and planar slicing on Gregory GB patches. The patches have been coloured by valency and the outlines of the patches are depicted. Polygons of the input meshes from top to bottom: 20 triangles, 20 quads, 12 pentagons and 120 hexagons; and 6 quads and 12 hexagons.

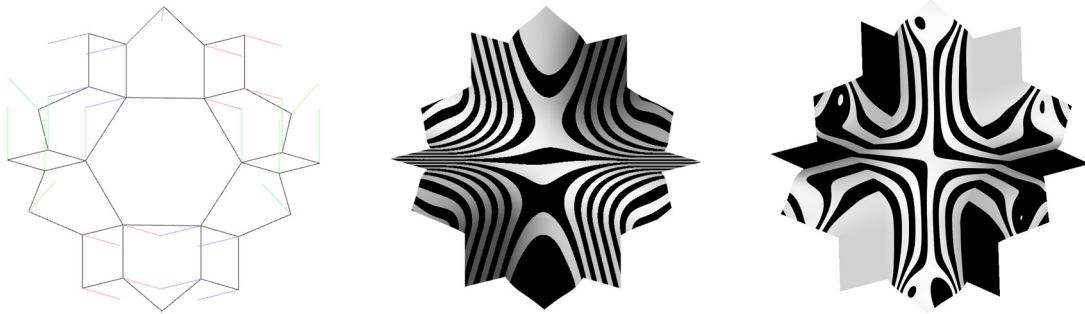


**Fig. 13.** A hexagonal Gregory GB patch smoothly joined to pentagonal and quadrilateral Gregory S-patches. Input mesh and normals (left), planar slicing (middle) and reflection lines (right) on the resulting surfaces.

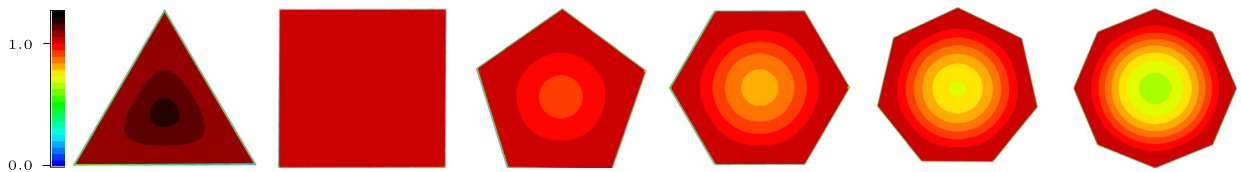


**Fig. 14.** Sum of the basis functions of cubic GB patches on regular polygons. Weight excess occurs in the triangular case and the functions sum to unity everywhere on the square. The rest of the polygons exhibit weight deficiency.

## References

- Boschirolì, M., Fünzig, C., Romani, L., Albrecht, G., 2012.  $G^1$  rational blend interpolatory schemes: a comparative study. *Graph. Models* 74 (1), 29–49.
- Boubekeur, T., Alexa, M., 2008. Phong Tessellation. *ACM Trans. Graph.*, vol. 27. ACM, p. 141.
- Chiyokura, H., 1986. Localized surface interpolation method for irregular meshes. In: *Advanced Computer Graphics*. Springer, pp. 3–19.
- Chiyokura, H., Kimura, F., 1983. Design of solids with free-form surfaces. *ACM SIGGRAPH Comput. Graph.* 17 (3), 289–298.
- Clough, R.W., Tocher, J.L., 1965. Finite element stiffness matrices for analysis of plates in bending. In: *Conference on Matrix Methods in Structural Mechanics*. Wright Patterson Air Force Base, Ohio, pp. 515–545.
- Farin, G., 1982. A construction for visual  $C^1$  continuity of polynomial surface patches. *Comput. Graph. Image Process.* 20 (3), 272–282.
- Farin, G., 1986. Triangular Bernstein-Bézier patches. *Comput. Aided Geom. Des.* 3 (2), 83–127.
- Floater, M.S., 2015. Generalized barycentric coordinates and applications. *Acta Numer.* 24, 161–214.
- Fünzig, C., Müller, K., Hansford, D., Farin, G., 2008. PNG1 triangles for tangent plane continuous surfaces on the GPU. In: *Proceedings of Graphics Interface 2008*. Canadian Information Processing Society, pp. 219–226.
- Gregory, J.A. *Smooth Interpolation Without Twist Constraints*. Brunel University Mathematics Technical Papers collection, 1974.
- Gregory, J.A., Lau, V.K., Zhou, J., 1990. Smooth parametric surfaces and  $n$ -sided patches. In: *Computation of Curves and Surfaces*. Springer, pp. 457–498.
- Hall, R., Mullineux, G., 1999. The Zheng-Ball construction without twist constraints. *Comput. Aided Geom. Des.* 16 (3), 165–175.
- Hettinga, G.J., Kosinka, J., 2017. Phong tessellation and PN polygons for polygonal models. In: *EG 2017 – Short Papers*. The Eurographics Association.



- Hettinga, G.J., Barendrecht, P.J., Kosinka, J., 2018. A comparison of GPU tessellation strategies for multisided patches. In: EG 2018 – Short Papers. The Eurographics Association.
- Karčiauskas, K., Peters, J., 2017. Improved shape for refinable surfaces with singularly parameterized irregularities. *Comput. Aided Des.* 90 (Supplement C), 191–198. SI:SPM2017.
- Langer, T., Belyaev, A., Seidel, H.-P., 2008. Mean value Bézier maps. In: *International Conference on Geometric Modeling and Processing*. Springer, pp. 231–243.
- Leung, Y.-S., Wang, C.C., Zhang, Y., 2011. Localized construction of curved surfaces from polygon meshes: A simple and practical approach on GPU. *Comput. Aided Des.* 43 (6), 573–585.
- Lodha, S., 1993. Filling  $N$ -sided holes. In: *Modeling in Computer Graphics*. Springer, pp. 319–345.
- Longhi, L., 1986. Interpolating Patches between Cubic Boundaries. University of California, Computer Science Division, Berkeley.
- Loop, C.T., DeRose, T.D., 1989. A multisided generalization of Bézier surfaces. *ACM Trans. Graph.* 8 (3), 204–234.
- Loop, C., DeRose, T.D., 1990. Generalized B-spline surfaces of arbitrary topology. *SIGGRAPH Comput. Graph.* 24 (4), 347–356.
- Malraison, P., 2000.  $N$ -Sided Surfaces: A Survey. Technical report. Spatial Technology Inc Boulder Co.
- Salvi, P., Várady, T., 2014.  $G^2$  surface interpolation over general topology curve networks. In: *Computer Graphics Forum*, vol. 33. Wiley Online Library, pp. 151–160.
- Salvi, P., Várady, T., 2016. Multi-sided surfaces with fullness control. In: *Proceedings of the Eighth Hungarian Conference on Computer Graphics and Geometry*, pp. 61–69.
- Schäfer, H., Nießner, M., Keiner, B., Stamminger, M., Loop, C., 2014. State of the art report on real-time rendering with hardware tessellation. In: *Eurographics 2014 – State of the Art Reports*. The Eurographics Association.
- Shirman, L.A., Séquin, C.H., 1987. Local surface interpolation with Bézier patches. *Comput. Aided Geom. Des.* 4 (4), 279–295.
- Shirman, L.A., Séquin, C.H., 1991. Local surface interpolation with Bézier patches: errata and improvements. *Comput. Aided Geom. Des.* 8 (3), 217–221.
- Várady, T., Rockwood, A., Salvi, P., 2011. Transfinite surface interpolation over irregular  $n$ -sided domains. *Comput. Aided Des.* 43 (11), 1330–1340.
- Várady, T., Salvi, P., Karikó, G., 2016. A multi-sided Bézier patch with a simple control structure. In: *Computer Graphics Forum*, vol. 35. Wiley Online Library, pp. 307–317.
- Várady, T., Salvi, P., Kovács, I., 2017. Enhancement of a multi-sided Bézier surface representation. *Comput. Aided Geom. Des.* 55, 69–83.
- Vlachos, A., Peters, J., Boyd, C., Mitchell, J.L., 2001. Curved PN triangles. In: *Proceedings of the 2001 symposium on Interactive 3D graphics*. ACM, pp. 159–166.
- Wachspress, E., 1975. *A Rational Finite Element Basis*. Academic Press.
- Wang, W., Jüttler, B., Zheng, D., Liu, Y., 2008. Computation of rotation minimizing frames. *ACM Trans. Graph.* 27 (1), 2.
- Zheng, J., 2001. The  $n$ -sided control point surfaces without twist constraints. *Comput. Aided Geom. Des.* 18 (2), 129–134.
- Zheng, J., Ball, A.A., 1997. Control point surfaces over non-four-sided areas. *Comput. Aided Geom. Des.* 14 (9), 807–821.